Atmospheric Research 334 (2026) 108752

Contents lists available at ScienceDirect

Atmospheric Research

journal homepage: www.elsevier.com/locate/atmosres

Associations between the thermal spring timing variability and atmospheric teleconnection patterns over the past six decades in Finland

Sadegh Kaboli [a,*], Ville Kankare [a,b], Ali Torabi Haghighi [c], Cintia Bertacchi Uvo [d,e], Elina Kasvi [a]

[a] Department of Geography and Geology, University of Turku, Finland
[b] Finnish Geospatial Research Institute (FGI), National Land Survey of Finland, Finland
[c] Water, Energy and Environmental Engineering Research Unit, Faculty of Technology, University of Oulu, Finland
[d] Finnish Environment Institute, Finland
[e] Division of Water Resources Engineering, Lund University, Sweden

ARTICLE INFO

Keywords:
Atmospheric teleconnection patterns
Global warming
Thermal seasons
Boreal regions
Finland

ABSTRACT

The timing of the spring season in the boreal region is shifting under global warming, with profound impacts on ecosystems and hydrological processes. However, the mechanisms driving this transition and its considerable interannual variability are not well described, especially regarding the influence of large-scale atmospheric teleconnection patterns. This study examines the temporal variability of the observed thermal spring season across Finland, a boreal country warming faster than the global average. Key spring timing indices, including onset, end, duration, and growing season onset, were calculated and analyzed using high-resolution (1 km × 1 km) daily mean temperature data from 1961 to 2023. Spatial and temporal patterns were identified through Empirical Orthogonal Function (EOF) decomposition, and their associations with major atmospheric teleconnection patterns were examined. Results indicated that during the past six decades, the spring onset has advanced by 2–6 days/decade, with the most pronounced changes in the coastal and southwestern parts of the country. The duration of the spring season has extended by 3–6 days/decade in the northern areas and along the southwestern coast. The early spring onset was associated with a strong positive phase of the Arctic Oscillation (AO), and delayed spring end and growing season onset were linked to the positive phase of the East Atlantic–West Russia (EAWR) pattern. By contrast, an early growing season start was linked to the positive phase of the North Atlantic Oscillation (NAO). The duration of the thermal spring season showed a strong association with the Scandinavian (SCA) pattern.

1. Introduction

Global warming has exhibited a successive decadal increase in global temperature; over the past four decades, each consecutive decade has been warmer than any preceding one since 1850 (Intergovernmental Panel on Climate Change (IPCC), 2023). Ongoing global warming is altering the seasonal climatological cycle worldwide, leading to shifts in the onset, end, and duration of thermal seasons (Lin and Wang, 2022). Investigating the seasonal cycle characteristics under climate change, including their timing and intensity, has gathered increasing attention in recent scientific publications (Zhu et al., 2025; Jo et al., 2024; Hekmatzadeh et al., 2020), as it has a wide range of influences on regional ecosystem services, farming practices, and socio-economic attributes (Parmesan, 2006).

Global warming has also altered the seasonal cycle in the boreal region, particularly affecting the timing of spring. Spring is especially important among all thermal seasons, as it marks the onset of snowmelt, a process that regulates the hydrological cycle (Wu et al., 2018). Spring is a critical period when nature rejuvenates, animals migrate, insects emerge, and generally, it affects both fauna and flora, and consequently, human life (Ren et al., 2024; Ault et al., 2011). As a consequence of anthropogenic climate change, the transition into summer has accelerated and winters have become shorter, leading to reduced snow cover, shorter ice periods, earlier and smaller spring floods, and higher winter discharges (Olsson et al., 2015; Luomaranta et al., 2014). Additionally, the growing season has undergone significant alterations in its onset, termination, and overall duration. Over the last 50 years, the length of the growing season in Europe has increased by approximately 5 days per

* Corresponding author at: Department of Geography and Geology, University of Turku, Vesilinnantie 5, FI-20014 Turku, Finland.
E-mail address: sadegh.kaboli@utu.fi (S. Kaboli).

https://doi.org/10.1016/j.atmosres.2026.108752
Received 14 October 2025; Received in revised form 17 December 2025; Accepted 5 January 2026
Available online 6 January 2026

decade (Cornes et al., 2019). This shift in spring timing disrupts forests and agricultural cycles, affecting crop yields and food security (Ghag et al., 2024; Seidl et al., 2017). Furthermore, the timing of biological events, such as plant blooming and animal migrations, may be misaligned, leading to ecological imbalances (Vaitkuviene et al., 2015; Linkosalo et al., 2009).

In Finland, climate change has altered the seasonal cycle of temperature-driven phenomena. According to Luomaranta et al. (2019), winters are characterized by reduced snow depth and shorter ice duration. The growing season has become longer and warmer (Aalto et al., 2023), the number of frost days in spring has decreased, and spring snowmelt floods now occur earlier (Lintunen et al., 2024; Aalto et al., 2023). Furthermore, Okkonen and Kløve (2010) reported that reduced groundwater levels in spring and decreased river baseflow in summer are expected, which increases the risk of summer drought. Therefore, these changes have raised environmental concerns and highlighted the need for adaptation in sectors such as agriculture, infrastructure, and ecosystem management within the boreal zone.

However, natural climate variability also contributes to the interannual and decadal dynamics of thermal indices, the large-scale atmospheric teleconnection patterns playing a key role (Naderian et al., 2025; Irannezhad and Kløve, 2015; Jaagus et al., 2003). In the context of Finland, several studies have demonstrated this influence. For instance, atmospheric circulation patterns have been identified as important explanatory factors for climatological drought variability in the country (Irannezhad et al., 2017). Additionally, research on the operating season of the Oulu–Hailuoto ice road has shown that both the start and end of the season are linked to freezing and thawing degree-days, which are also influenced by atmospheric teleconnection patterns (Kiani et al., 2018).

Other critical factors of the natural variability include latitude, altitude, distance from coastlines, and vegetation cover, which modulate local thermal responses to broader climatic factors (Aalto et al., 2022; Deng et al., 2019). As indicated by both climatological data and remotely sensed phenological indices, spring season timing variation has exhibited consistent annual fluctuations that are spatially coordinated across regions (Schwartz et al., 2006; Cayan et al., 2001). This synchronization suggests that the onset of spring may be influenced by specific modes of climate variability, and it motivates an analysis of the relationship between variations in thermal spring timing and regional climatological patterns, which can provide insights into the drivers of thermal spring dynamics.

Therefore, to be able to make region-specific predictions and plan effective adaptation strategies, it is crucial to better understand the factors driving spring dynamics, what part of the variation is due to natural environmental factors and teleconnection patterns, and what can be attributed to anthropogenic climate change. This requires identifying the relationship between thermal spring timing variability and regional climatological modes, alongside a thorough evaluation of long-term changes that cannot be attributed to natural variability.

In this study, we investigate the timing of the boreal thermal spring season, its interannual associations with atmospheric teleconnection patterns, and its long-term changes related to anthropogenic climate change, using high-resolution temperature observations across Finland over the past 6 decades. First, we examine how the timing of the thermal spring season changed across Finland during the period 1961–2023. Second, we investigate the relationship between the dominant modes of spring timing variability and large-scale atmospheric teleconnection patterns. Third, we classify geographical regions based on their spring timing characteristics to identify spatial patterns and regional distinctions.

2. Materials and methods

2.1. Study area

Finland, located in northern Europe, covers an area of approximately 338,000 km^2. It extends 1150 km from south to north within the boreal environment. The country lies approximately between 59° and 70° N latitude and 20° and 32° E longitude (Fig. 1). The topography in Finland is generally flat, gradually increasing from the western coast to the east. However, in the north, the terrain elevation is connected to the Scandinavian Mountains, which represent the highest elevations in the country (Fig. 1b). Lakes are prominent, especially in the central and eastern parts of the country, influencing climatic variations in the region. The climate in Finland is generally categorized as boreal, characterized by cool, short summers in most areas and mild, warm summers in the southernmost region (Olsson et al., 2015; De Castro et al., 2007). Long-term averages of annual mean temperature indicate a natural decrease in temperature from south to north (Fig. 1c). Similarly, annual precipitation decreases from south to north (Pirinen et al., 2012).

Finland's climate is shaped by its unique geographical setting. The Arctic Ocean to the north and the Baltic Sea to the south and west influence the regional temperature and precipitation patterns (Aalto et al., 2016). In addition, factors such as the high latitudes, the Scandinavian Mountains chain, and the proximity of the extensive Eurasian landmass further modulate the country's climatic conditions.

2.2. Data

2.2.1. Climatological data

This study's gridded daily mean air temperature data are sourced from the Finnish Meteorological Institute (FMI). The datasets used in this study span the period from 1961 to 2023 and cover the entirety of Finland at a 1 × 1 km spatial resolution. The gridding process is based on the geostatistical prediction of observational data collected from stations in Finland and neighboring countries. The interpolation model has been refined and enhanced using various external predictors, including latitude, longitude, lake cover, elevation, proximity to the sea, and relative elevation. A detailed description of this comprehensive data generation process and methodology is provided by Aalto et al. (2016).

2.2.2. Teleconnection data

This study examines the six most influential teleconnection patterns (TCPs, Table 1) affecting the Nordic regions, particularly Finland, as identified in previous research (Naderian et al., 2025; Irannezhad and Kløve, 2015). The characteristics of these patterns are summarized in Table 1.

Since atmospheric teleconnection patterns influence air temperature almost immediately and without significant lag, each TCP index was calculated by averaging the monthly values over the months corresponding to each timing index (Irannezhad and Kløve, 2015). The corresponding months for each index are discussed in more detail in Section 2.3.2.

2.3. Methods

2.3.1. Definition of the spring season timing indices

To investigate the temporal dynamics of the thermal spring season, region-specific temperature thresholds were used (Ruosteenoja et al., 2020). We employed four timing indices to define the spring timing: Spring Season Onset (SSO), Growing Season Onset (GSO), Spring Season End (SSE), and Spring Season Duration (SSD). SSO, GSO, and SSE are determined using the temperature deviation integral method (Ruosteenoja et al., 2016), which is widely used by researchers in boreal countries (Aalto et al., 2022; Ruosteenoja et al., 2020). Using this approach, the thermal season onset can be determined by finding the absolute minimum point of the time integral as follows:

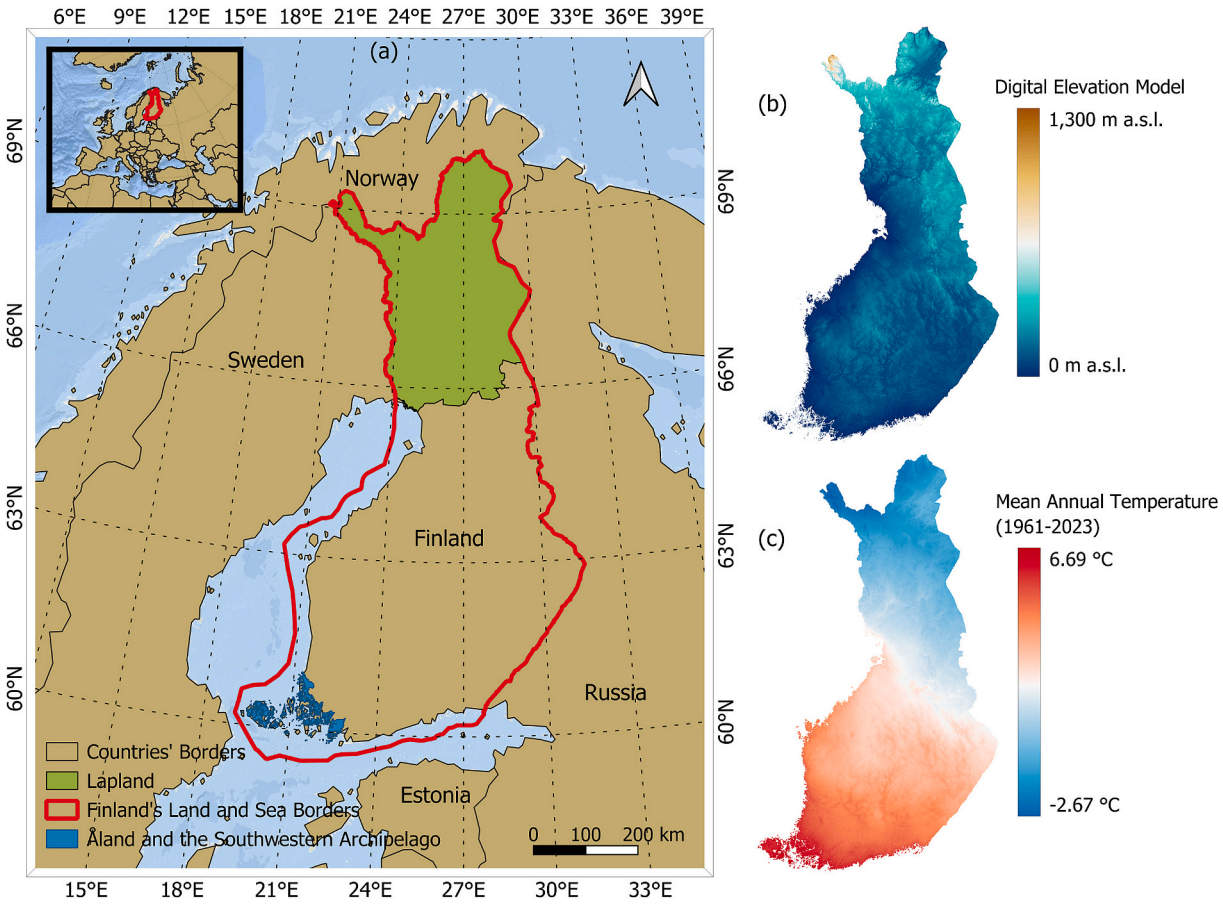

Fig. 1. Overview of Finland's geographical and climate characteristics. (a) Map of Finland and its neighboring countries, with key internal regions highlighted, including Lapland and Southwestern Archipelago; (b) digital elevation model (meters above sea level); (c) long-term average of annual mean temperature from 1961 to 2023 (°C).

$$I = \int_{t_0}^{t} (T - T_{base})dt \quad (1)$$

This approach (eq. 1) utilizes daily mean temperature data and a fixed thermal threshold (T_{base}) as the base temperature for defining the start of the season. The initial date, t_0, is considered to be the first of January. However, if the temperature on the first of January is higher than T_{base}, the first date when the temperature falls below T_{base} is considered t_0.

We defined the beginning of the summer season as the termination of the spring season. The base temperatures (T_{base}) used to identify the onset of spring and summer are 0 °C and 10 °C, respectively (Finnish Meteorological Institute, 2025a). After determining the onset and end dates of the spring season, we considered the number of days between them as the spring season duration (SSD).

Within the spring season, an important timing characteristic is the start of the growing season, calculated using a base temperature of 5 °C. This threshold, which is widely applied in studies of the Nordic region (Ruosteenoja et al., 2020), is additionally considered in this study as an indicator of the midpoint of the thermal spring season.

2.3.2. Identification of corresponding months for each timing index

The timing associated with each thermal spring index, including SSO, GSO, and SSE, was determined using box plots that depict the 10th and 90th percentiles of each index across Finland from 1961 to 2023 (Fig. 2). Considering the whole country, over the past six decades, the 10th and 90th percentile dates for SSO occurred on the 79th and 120th days of the year, respectively. For GSO, these dates correspond to the 110th and 145th days, and for SSE, to the 130th and 167th days. Based on these thresholds, the mean values of each standardized teleconnection index were calculated for four distinct periods: (1) March–April, representing the onset of spring; (2) April–May, corresponding to the spring midpoint or the onset of the growing season; (3) May–June, associated with the end of spring; and (4) March–June, encompassing the full duration of the spring season.

2.3.3. Identifying spatial and temporal patterns of spring dynamics

We used the Empirical Orthogonal Function (EOF) method to identify the dominant modes of variability in the timing indices. This method (Lorenz, 1956) is useful for simplifying the interpretation of annual meteorological variability by capturing the majority of meteorological variability with just a few orthogonal spatial modes (Lin et al., 2022).

EOF technique has three components: eigenvectors, which represent the spatial patterns (EOFs); eigenvalues, which indicate the variance explained by each mode; and corresponding principal components (PCs) time series. To obtain all these parameters, the annual index values were first calculated as described in the Section 2.3.1, after which EOF analysis was performed using the Climate Data Toolbox for MATLAB (Greene et al., 2019). We used the North significance test (North et al., 1982) to separate significant physical signals from noise in the estimated spatial patterns.

2.3.4. Spatial clustering of spring duration

To examine regional variations in the duration of the spring season, K-means clustering was applied to the annual standardized SSD time series across all grid points to identify regions exhibiting coherent spring-duration characteristics over time. Dimensionality-reduction approaches such as EOF truncation retain only the leading high-

Table 1
Summary of the Considered Climatological Teleconnection Patterns (TCP).

Teleconnection	Action Center	Positive Phase	Reference
North Atlantic Oscillation (NAO)	Ponta Delagada (Azores) and Stykkisholmur (Iceland).	Intensifies the westerly flow and directs warm and moist air toward northern Europe, with high pressure over the Azores and low pressure near Iceland.	(Fabiano et al., 2020; Hurrell, 1995)
East Atlantic (EA)	North Atlantic from east to west.	Results in positive temperature anomalies in Europe, with high pressure over Western Europe and low pressure over the subpolar North Atlantic.	(CPC, 2012; Barnston and Livezey, 1987)
East Atlantic/ West Russia (EAWR)	North Atlantic, northern China, north of the Caspian Sea, and Europe.	Causes negative temperature anomalies over western Russia, with high pressure over Europe and northern China, and low pressure over the northern Caspian Sea and the central North Atlantic.	(CPC, 2012; Barnston and Livezey, 1987)
Scandinavia (SCA)	Over Scandinavia, with less intense centers of reverse sign over eastern Russia/western Mongolia and western Europe.	Causes drier air to flow toward Finland, with high pressure over Scandinavia and low pressure over eastern Russia and western Europe.	(Bueh and Nakamura, 2007; Barnston and Livezey, 1987)
Polar/Eurasia (POL)	Over the polar region, as well as northern China and Mongolia	Causes positive temperature anomalies in eastern Siberia, with high pressure over northern China and Mongolia and low pressure over the polar region.	(CPC, 2012)
Arctic Oscillation (AO)	A dipole pattern spans between the polar cap and the adjacent zonal belt centered around 45°N.	Causes more humid and warmer weather in Scandinavia, with high pressure in the adjacent zonal belt centered around 45°N and low pressure in the polar cap.	(Thompson and Wallace, 1998)

variance components of the field, which may suppress low-variance temporal features that can still be scientifically important. Using the complete dataset for clustering ensures that all temporal information at each grid cell is preserved (Kuschnerus et al., 2021).

This approach grouped grid points into K distinct clusters by minimizing intra-cluster variability and identifying regions with similar temporal patterns in spring duration. The classical K-means clustering technique (Lloyd, 1982; MacQueen, 1967), which is an unsupervised nonhierarchical algorithm, was performed using the squared Euclidean distance metric with 10 random initializations of the centroids and a maximum of 500 iterations to ensure stable clustering results. To determine the optimal number of clusters in a range of 1 to 15 clusters (K), the Elbow method was employed by plotting the sum of squared errors between sample points within each cluster and the cluster centroid. The elbow is the point at which adding more clusters does not significantly improve the model.

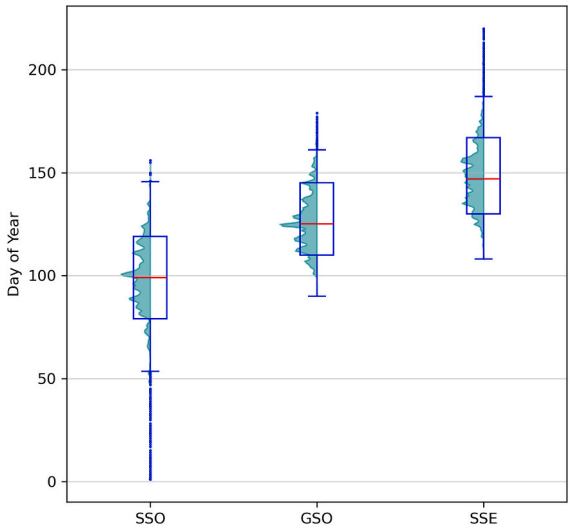

Fig. 2. Box plots of Spring Onset, Growing Season Onset, and Spring End across Finland (1961–2023). Boxes represent the 10th to 90th percentiles range, with the red line indicating the median. Whiskers extend to 1.5 times the interquartile range (25th–75th percentiles), and points beyond this range are shown as outliers. The green histogram shows the frequency distribution of the indices across Finland from 1961 to 2023. (For interpretation of the references to colour in this figure legend, the reader is referred to the web version of this article.)

Since the subjective methods, such as the Elbow method alone, may be insufficient for the selection of the optimum number of K in high-resolution gridded samples (Zhang et al., 2016), we complemented it with the Silhouette method (Rousseeuw, 1987) to enhance the accuracy of cluster selection. Silhouette scores range from −1 to +1, representing the quality of a sample's position within its cluster, with −1 and + 1 representing a poor and a good fit, respectively. Zero values in this index indicate neutrality toward any cluster. The average silhouette score, along with box plots showing the 25th and 75th percentiles of all scores, was used to determine the optimum number of clusters.

2.3.5. *Trend detection in spring season dynamics*

The Mann-Kendall significance test (Kendall, 1957; Mann, 1945) and Sen's slope method (Sen, 1968) were employed to detect significant trends and calculate the slope of change on a grid-by-grid basis. Additionally, the Pettitt test (Pettitt, 1979) was applied to identify potential change points within the time series.

In this study, a confidence level of 95 % ($p < 0.05$) was used to identify statistically significant trends in the time series. These nonparametric statistical methods are commonly applied in various climatic studies at both station-based and pixel-based spatial resolutions (Naderian et al., 2025; Zhao et al., 2024; Kaboli et al., 2021; Sobral et al., 2019). One advantage of these nonparametric approaches is that the data do not need to follow a specific distribution. However, positive autocorrelation in time series can increase the likelihood of incorrectly rejecting the null hypothesis of no trend (Yue et al., 2002; Serinaldi and Kilsby, 2016). To address this issue, we employed the trend-free pre-whitening method (TFPW) (Yue et al., 2002) before conducting trend, slope, and change point analyses to detect and remove any existing autocorrelation in the time series.

3. Results

3.1. Long-term variability and trends of spring timing characteristics

The temporal average of gridded spring timing indices (1961–2023) revealed a south-to-north gradient for SSO, GSO, and SSE. This spatial pattern reflects the extensive latitudinal gradient across Finland, with earlier occurrences of the spring timing indices in the southern regions and progressively later occurrences toward the north (Fig. 3). Based on the multi-year average, spring typically started earliest in the southwestern areas, including the Åland Islands, around early March, while the latest onset occurred in high Lapland around late April (Fig. 3a). Conversely, spring usually ended by mid-May in the southern regions but extended until approximately early July in northern Lapland (Fig. 3c). The GSO followed a similar south-to-north pattern, occurring around late April in the south and reaching its latest timing in the northern and northwestern areas around the third week of May (Fig. 3b).

Across most of Finland, particularly in the central regions between 62° and 68°N, excluding the western coastal areas, the long-term average duration of the spring season was approximately 50 days. However, in high Lapland, where the influence of the Arctic Ocean on regional temperature has been documented (Aalto et al., 2016), spring lasted around 60 days. The longest spring durations, exceeding 80 days, occurred in the southwestern coastal areas and the Åland Islands (Fig. 3d).

Based on the analysis of this study, the timing of spring shifted earlier across most of Finland over the past six decades, with the greatest changes observed in the southern and southwestern regions. The grid-based temporal trend analysis across Finland revealed a predominantly negative trend for SSO, GSO, and SSE over the past 63 years (Fig. 3e–g). Among all indices, the highest rates of change were observed in the southern and southwestern regions of the country (Fig. 3e–h). SSO in the south and southwestern coastal regions exhibited a statistically significant decreasing trend, with a rate of 2 to 6 days per decade (Fig. 3e). In contrast, the rate of change in the eastern regions, particularly between latitudes 60° and 63°N, was the lowest and not statistically significant. In Lapland, the negative trend was also statistically significant, ranging from approximately 2 to 4 days per decade, except in central northern Lapland, where the trend was less pronounced.

High rates of change in GSO were observed along the southern and western coasts, with a negative trend of approximately 1 to 3 days per decade (Fig. 3f). A comparable negative trend was also detected in Lapland, with stronger rates in the northern areas. In most central regions of the country, mostly between latitudes 62° and 65°N, GSO showed only a weak negative shift, which was not statistically significant at the 95 % confidence level.

The SSE exhibited a negative trend across most of the study area; however, the trends were largely significant in the central and southern regions, the coastal areas, and parts of the high-elevation northwest of Lapland (Fig. 3g). In these regions, the shift ranged from 1 to 3 days per decade.

The trends in SSD grid points were predominantly positive,

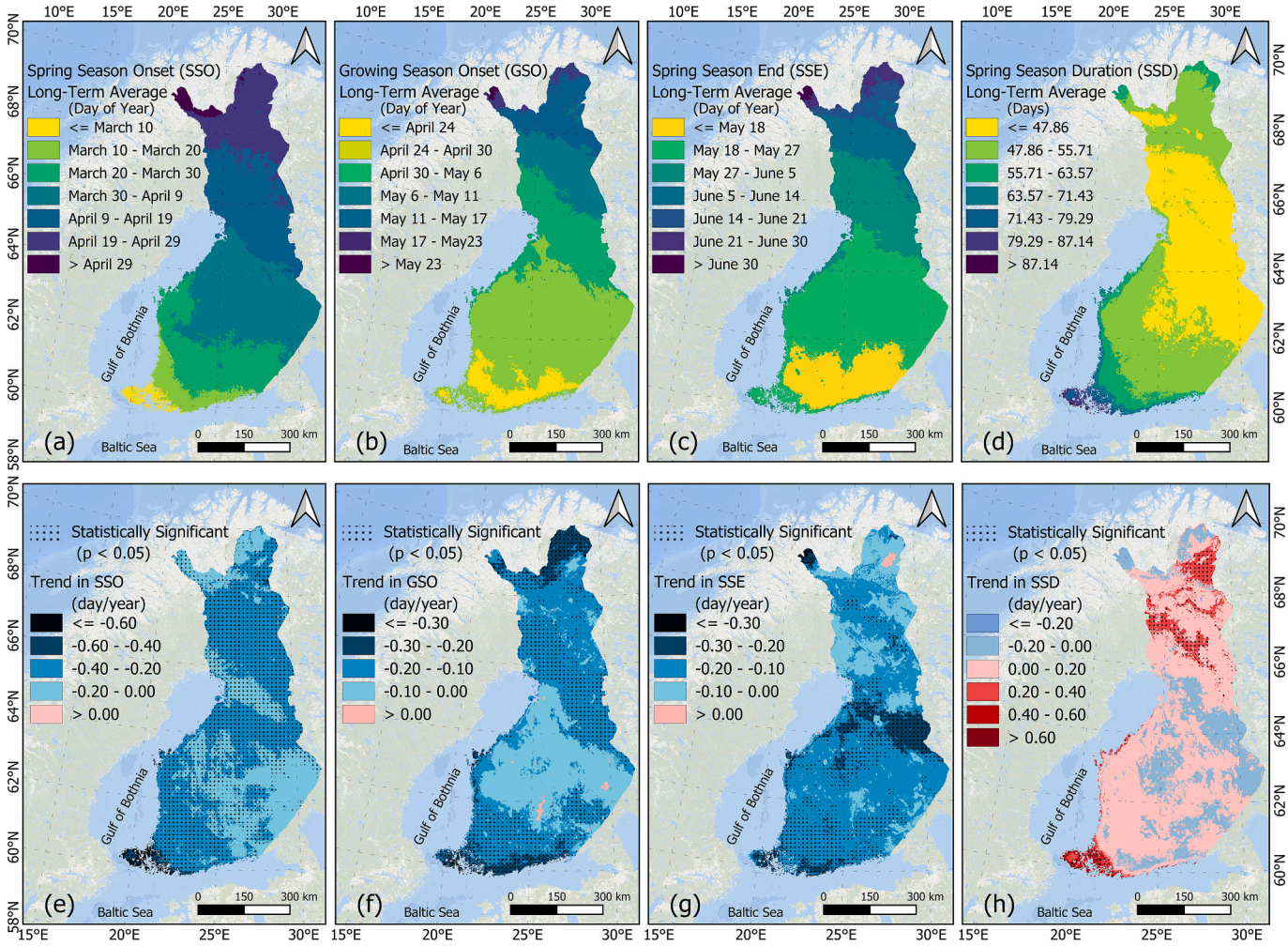

Fig. 3. Long-term averages (1961–2023) of (a) SSO, (b) GSO, (c) SSE, and (d) SSD and grid-based temporal trend analysis using the Mann-Kendall test and Sen's slope for (e) SSO, (f) GSO, (g) SSE, and (h) SSD across Finland for the period 1961–2023.

particularly in the northern region, especially north of 66°N (Fig. 3h), as well as in the southwestern islands and coastal areas. Although trends are not statistically significant in the majority of the country, the magnitude of the statistically significant trends varied from 2 days per decade in Lapland to 6 days per decade in the southwestern islands (Fig. 3h).

3.2. *Leading modes of spring timing variability and their linkage to atmospheric teleconnection patterns*

EOF analysis captured the leading modes of variability in spring timing indices by analyzing anomalies from the mean through covariance matrix decomposition. The first three EOFs for each timing index collectively explained at least 70 % of the total variance (Fig. 4a–l) and were retained for further analysis. All three modes are statistically distinct from each other and do not form a degenerate pair based on the results of the north test, as the error intervals of the adjacent eigenvectors do not overlap (Fig. S1a–d; Supplementary Information).

The interannual variability corresponding to these spatial modes was illustrated as time series in Fig. S2a–d for the first three modes, and separately in Fig. 5 for the first mode. To assess the physical relevance of the EOF maps identified in this study to the spring timing variables, we examined the spatial patterns of the timing indices associated with different intervals of PC1. For each index, we mapped the average spring timing values for time steps below the 10th percentile of PC1 (low scores), and for time steps above the 90th percentile of PC1 (high scores) (Fig. S3a–h). The resulting spatial patterns resembled the leading EOF structures. For example, for SSO (Figs. S3a and S3b), the fields associated with low PC1 scores reproduced the characteristic EOF1 pattern (Fig. 4a) and showed substantially earlier spring onset across southern regions, consistent with the dominant EOF1 map. The map representing the upper end of the PC1 distribution (Fig. S3b) displayed a gradual south-to-north gradient, which further confirms the EOF1 structure (Fig. 4a). Similar agreement between the EOF1 patterns and the 10th- and 90th-percentile composites is observed for the remaining indices, including GSO, SSE, and SSD (Fig. S3c–h). This coherence supports the physical reality of the principal components identified in this study.

The onset of spring exhibited a clear south-to-north shift, with accelerated changes in southern Finland beginning in the late 1980s (Figs. 4a and 5a). The dominant spatial mode of variability in spring onset dates, represented by EOF1, accounted for approximately 45 % of the total variance. Although the pattern revealed a uniform directional shift across the study area, southern regions exhibited more than twice the magnitude of shift compared to northern regions (Fig. 4a). In contrast, the second mode (EOF2) explained approximately 20 % of the variance and highlighted an opposing directional trend between the southern and northern grid points (Fig. 4b).

The spatial patterns of GSO and SSE were similar, with EOF1 explaining 48.38 % and 45.35 % of the total variance, respectively (Fig. 4d, g). Both indices exhibited a comparable shift across the country, with higher intensity in the central regions. In contrast, the EOF2 spatial patterns for both indices showed two distinct zones (Fig. 4e, h),

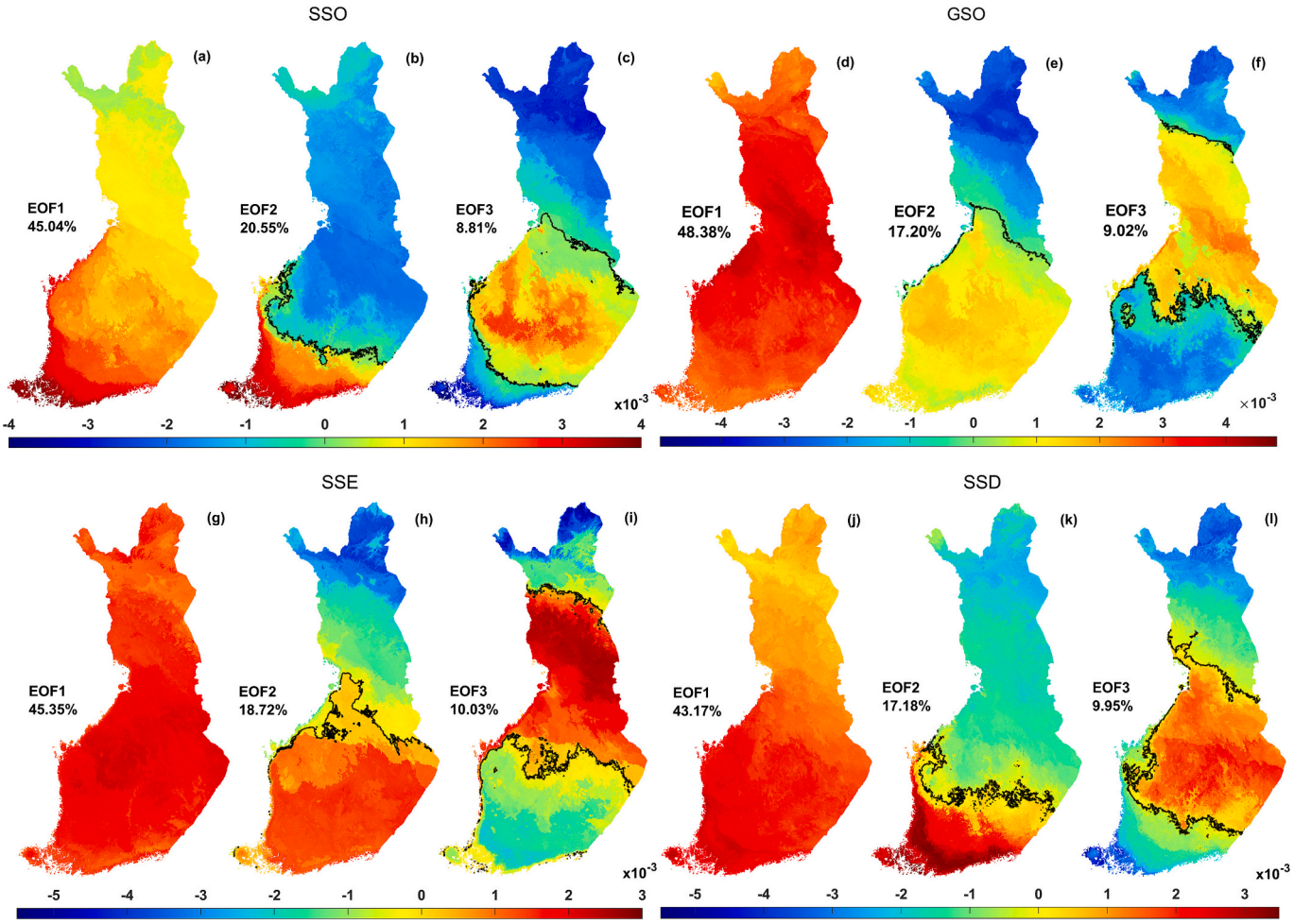

Fig. 4. Spatial pattern of EOF1 (a, d, g, j), EOF2 (b, e, h, k), and EOF3 (c, f, i, l) for SSO, GSO, SSE, and SSD across Finland; the black thick line represents where the grids' direction shifts from positive (red grid points) to negative (blue grid points). (For interpretation of the references to colour in this figure legend, the reader is referred to the web version of this article.)

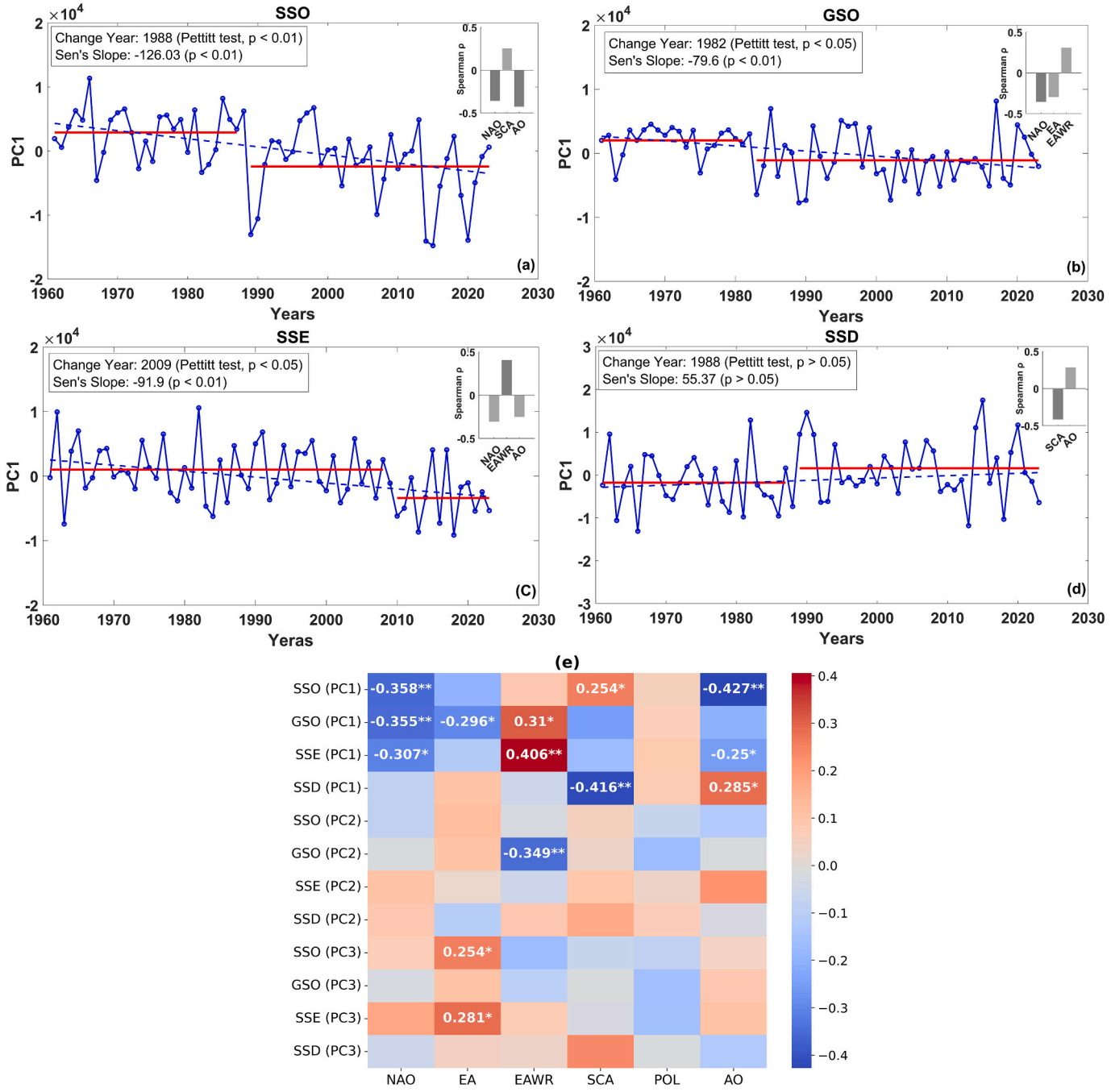

Fig. 5. Original time series of the first principal component (PC1) for (a) SSO, (b) GSO, (c) SSE, and (d) SSD during 1961–2023, showing abrupt change years (Pettitt test), trend lines (Sen's slope), and Spearman correlations with key teleconnection patterns (TCPs). Thick red lines indicate mean values before and after detected shifts. Bar charts display significant correlations: light gray ($p < 0.05$), dark gray ($p < 0.01$). (e) Spearman correlations between six TCPs and the first three PCs, with significance levels indicated as *$p < 0.05$ and **$p < 0.01$. (For interpretation of the references to colour in this figure legend, the reader is referred to the web version of this article.)

with one zone extending from the south to the center and an opposing zone from the center to the north. The SSD index exhibited positive values for all grid points in EOF1, which explained 43.17 % of the variance, with the highest values observed in the southern and southwestern regions (Fig. 4j). To further investigate the physical drivers of the identified EOF modes, we evaluated their spatial correlations with four key geographical characteristics: elevation, distance from the sea, latitude, and longitude. Among these factors, latitude displayed a relatively linear relationship with specific EOF patterns of the spring indices (Figs. S4j, S5k, and S7j), while the others demonstrated more complex spatial associations. Notably, latitude and elevation exhibited the strongest correlations with spring timing indices, as indicated by the Spearman correlation test (Figs. S4–7). These findings suggest that large-scale spatial gradients, particularly latitudinal and altitudinal influences, play an important role in shaping the observed patterns.

Fluctuations in the PC1 of the SSO (Fig. 5a) indicated that the dominant spatial pattern represented by EOF1 was not stationary but evolved over time. A statistically significant shift ($p < 0.01$) from a predominantly positive to a negative phase was detected using the Pettitt test, with the turning point identified in 1988. Additionally, the Sen slope estimator indicated a consistently strong negative trend over the study period ($p < 0.01$). This decreasing trend, particularly

pronounced in the southern and southwestern coastal areas, supports the grid-based temporal findings in the previous section on SSO.

PC1 analysis of the GSO and SSE revealed a significant downward trend ($p < 0.05$) from a positive to a negative dominant phase, with change points detected in 1982 for GSO and 2009 for SSE (Fig. 5b, c). The Sen's slope analysis further confirmed a strong negative trend ($p < 0.01$) for both indices over the study period. However, PC1 for the SSD indicated a non-statistically significant upward trend, with the upward tendency detected in 1988 (Fig. 5d).

Clear associations were revealed through Spearman correlation analysis between major TCPs and the time series of the first PCs of the spring timing indices. Earlier SSO was associated with the positive phases of the AO and the NAO (Fig. 5a), whereas delayed SSE was linked to the positive phase of the EAWR pattern (Fig. 5c). The growing season tended to start earlier under the influence of positive NAO and EA phases, and later under the positive EAWR pattern (Fig. 5b).

The strongest correlation was found between SSO dates and the AO index, with a correlation coefficient of −0.43 (Fig. 5e). Similarly, the standardized NAO index also exhibited a strong negative correlation with SSO over the past six decades, with a coefficient of −0.36 at the 0.01 significance level. These negative correlations suggest that strong positive phases of the NAO and AO tend to advance SSO in Finland. Conversely, a statistically significant positive correlation was found between SSO and the SCA at the 0.05 significance level, with a correlation coefficient of 0.25. This implies that the positive phase of the SCA may be associated with delayed spring onset.

SSE and GSO were positively correlated with the EAWR pattern, with correlation coefficients of 0.41 ($p < 0.01$) and 0.31($p < 0.05$), respectively. This correlation suggests that a robust positive phase of the EAWR is associated with a delayed end of the spring season and a later occurrence of the thermal growing season. In contrast, SSE and GSO showed significant negative correlations with the NAO index, with correlation coefficients of −0.31 ($p < 0.05$) and − 0.35 ($p < 0.01$), respectively (Fig. 5e).

PC1 of the spring season duration exhibited a strong negative correlation with the SCA ($r = -0.42$, $p < 0.01$) and a positive correlation with the AO ($r = 0.28$, $p < 0.05$) (Fig. 5e). These correlations suggest that a positive phase of the SCA and AO are associated with shorter and longer spring durations in Finland, respectively.

In general, PC2 and PC3 of the spring timing indices showed no strong significant correlations with TCPs, except that PC2 of GSO exhibited a relatively strong negative correlation with the EAWR pattern ($r = -0.35$, $p < 0.01$) (Fig. 5e). Notably, this correlation exhibited the opposite sign in the northern region, corresponding to negative grid values in the EOF2 map for GSO (Fig. 4e). The positive phase of the EA also showed weak positive relationships with the PC3 of SSO ($r = 0.25$, $p < 0.05$) and SSE ($r = 0.28$, $p < 0.05$). However, these coefficients were negative in the northern and southern parts of the country, based on the

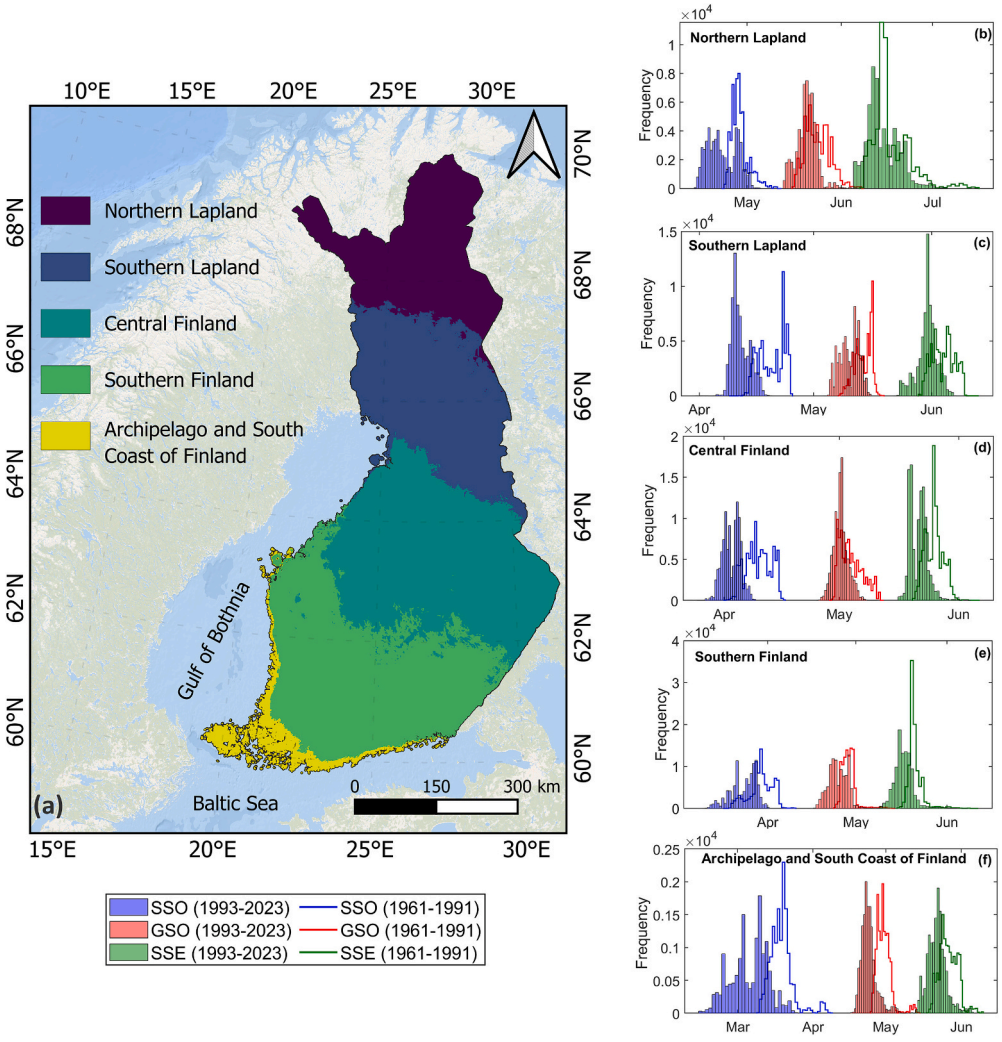

Fig. 6. Overview of regional clusters of spring season duration and the spatial histograms of indices for two time periods within each cluster. (a) Regional clusters of spring duration. (b-f) Spatial histograms depicting the average values of SSO, GSO, and SSE across two 31-year periods for the following clusters: (b) Northern Lapland; (c) Southern Lapland; (d) Central Finland; (e) Southern Finland; and (f) Archipelago and South Coast of Finland.

EOF3 patterns of SSO (Fig. 4c) and SSE (Fig. 4i).

3.3. Regional clustering of spring timing

To investigate regional differences in spring timing trends across Finland, spatial K-means clustering was applied to the annual standardized SSD time series from 1961 to 2023, which delineated five regions with distinct spring timing characteristics across Finland (Fig. 6a). The optimal number of clusters was determined using the elbow method, based on the sum of squared errors between the sample data and centroid values. Although the elbow point suggested five clusters, the smoothness of the graph made this determination less distinct (Fig. S8a). To validate this selection, silhouette scores were calculated. The 25th and 75th percentile box plots, along with the average silhouette scores, provided further support for five as the most suitable number of clusters (Fig. S8b).

The analysis of spring timing characteristics within each cluster revealed distinct regional variations in spring timing, with a gradual delay observed from the southern cluster to the northern cluster (Table 2). The Northern Lapland cluster showed the latest spring onset by late April, with a spring season duration of approximately 51 days and a standard deviation of 3.6 days (Table 2). The standard deviation in this cluster indicated relatively high spatial variability for SSE and SSD.

The Southern Lapland cluster extended approximately from 64°N to 67°N in northern Finland (Fig. 6a), with an SSD of around 47 days (Table 2). The lower standard deviation in this cluster suggests more consistent spring timing. The melting of the ice cover in the northern Bothnian Bay typically begins in early May and may persist until late May or early June (Finnish Meteorological Institute, 2025b). This prolonged ice cover delays coastal warming, causing the coastal temperature regime to align more closely with that of Southern Lapland. Consequently, this influence may explain the extension of this cluster toward the Bothnian coast (Fig. 6a).

The Central Finland cluster exhibited an SSD of approximately 47 days and a standard deviation of 1.9 days. The consistency of SSO, GSO, and SSE was highest in this cluster (Table 2). The Southern Finland cluster encompassed the inland areas of the southern part of the country. On average, spring lasted 53 days in this region, from late March to mid-May, and this cluster exhibited relatively high spatial variability in SSO.

The Archipelago and South Coast of Finland cluster was distinguished by the longest coastal stretch and included the highest number of coastal grid points compared to inland grid points (Fig. 6a). This cluster exhibited unique spring timing characteristics, with the longest mean SSD of 73 days, ranging from mid-March to late May, and the greatest standard deviation of 7.5 days among all clusters (Table 2).

To further explore and illustrate the consequences of the observed trends, spatial histograms of SSO, GSO, and SSE were computed as grid-wise temporal averages for two 31-year periods: 1961–1991 and 1993–2023, across all clusters (Fig. 6b–f). Overall, these spatial histograms highlight the ongoing shift toward earlier occurrences. Among all indices, the largest shift was observed in the SSO when comparing the spatial histograms between the two time periods, particularly in the Southern Lapland and Central Finland clusters (Fig. 6c, d). In contrast, shifts in the spatial frequencies of the spring timing indices between the two periods were relatively small in the Northern Lapland and Southern Finland clusters (Fig. 6b, e).

Further analyses were conducted on the time series derived from each cluster for each timing index to evaluate the consistency with the grid-based temporal analysis and the national-scale EOF analysis. Specifically, we calculated the correlation and trend of the area-averaged time series for each index within each cluster (Fig. 7).

Regional correlations derived from the time series of each cluster further confirmed the connections between AO, NAO, SCA, and EA with SSO (Fig. 7a–e); EAWR and NAO with GSO (Fig. 7a–c); NAO, AO, and EAWR with SSE (Fig. 7a–e); and SCA and AO with SSD (Fig. 7a–e). However, these analyses offered more detailed insights into the influence of the TCPs across different regions of the study area. For instance, earlier SSO timing, in the Southern Finland and Archipelago clusters, showed linkages to positive phases of the NAO and AO, with correlations of approximately −0.41 (Fig. 7d, e). However, the positive phase of the EA primarily affected the northern clusters, resulting in an earlier SSO ($r = -0.33$) (Fig. 7a).

The delayed GSO timing exhibited a connection to the positive phase of the EAWR in the Northern and Southern Lapland clusters ($r = 0.44$ and 0.39, respectively) (Fig. 7a, b). In contrast, the NAO was the most influential TCP for GSO in the Central Finland cluster (Fig. 7c), where its positive phase was associated with earlier GSO timing ($r = -0.33$). The earlier SSE timing in the Northern Lapland cluster was correlated with the positive phases of the NAO and AO (Fig. 7a), with correlation coefficients of approximately −0.33 and − 0.34, respectively. In contrast, the positive phase of the EAWR was the primary teleconnection pattern influencing the delayed SSE timing, in the central ($r = 0.40$) (Fig. 7c) and southernmost clusters ($r = 0.33$) (Fig. 7e).

SSD was linked to SCA across all clusters (Fig. 7a–e); however, this relationship was strongest in the Southern Lapland cluster and the southernmost cluster, where the positive phase of SCA led to a shorter SSD, with correlation coefficients of −0.42 and − 0.40, respectively. In this section, we focused on the correlations of the most influential TCPs ($p < 0.01$). For a comprehensive overview of correlations between all TCPs and spring timing indices across all clusters, see Fig. S9.

The long-term trends of each index within the clusters revealed the highest rates of change in the Archipelago and Southern Coast of Finland cluster, with SSO and SSD exhibiting the largest changes (Fig. 7j). SSO and GSO generally showed a significant negative trend across all clusters, except for GSO in central region (Fig. 7h). SSE also exhibited a negative trend, particularly in the central and southern clusters (Fig. 7h–j).

Assessment of the Pettitt test results for change point detection in the cluster-based time series revealed that 1988 was identified as the year of change for SSO, GSO, and SSD in the Archipelago and Southern Coast of Finland cluster (Fig. 7j). Changes were also observed in the late 1990s or early 2000s for SSO and GSO in the central and northern clusters (Fig. 7f–h); however, the SSO time series in the northernmost cluster exhibited a change point in the early 1980s (Fig. 7f). SSE exhibited different shift points at both the national scale, based on its fundamental mode, and at the cluster scale for the central and southernmost regions, with change points detected between the mid-2000s and late 2000s (Fig. 7h, j).

Table 2
Spatial mean and standard deviation of the temporal mean spring timing indices (SSO, GSO, SSE, and SSD) across clusters for the period 1961–2023.

Clusters	SSO (day of year)		GSO (day of year)		SSE (day of year)		SSD (days)	
	Mean	Std	Mean	Std	Mean	Std	Mean	Std
Northern Lapland	115.8 (April 26)	3.6	142.4 (May 21)	3.6	166.7 (June 16)	5.7	51	3.5
Southern Lapland	106.1 (April 16)	2.7	132.2 (May 11)	2.4	152.8 (June 2)	2.6	46.7	1.1
Central Finland	96.7 (April 7)	2.6	122.6 (May 1)	2.3	143.5 (May 23)	2.1	46.8	1.9
Southern Finland	85.8 (March 27)	4.4	116.7 (April 26)	2.6	139.1 (May 19)	2.7	53.3	3.8
Archipelago and South Coast of Finland	70.9 (March 12)	6.2	117.1 (April 26)	2.9	144.2 (May 24)	3.6	73.3	7.5

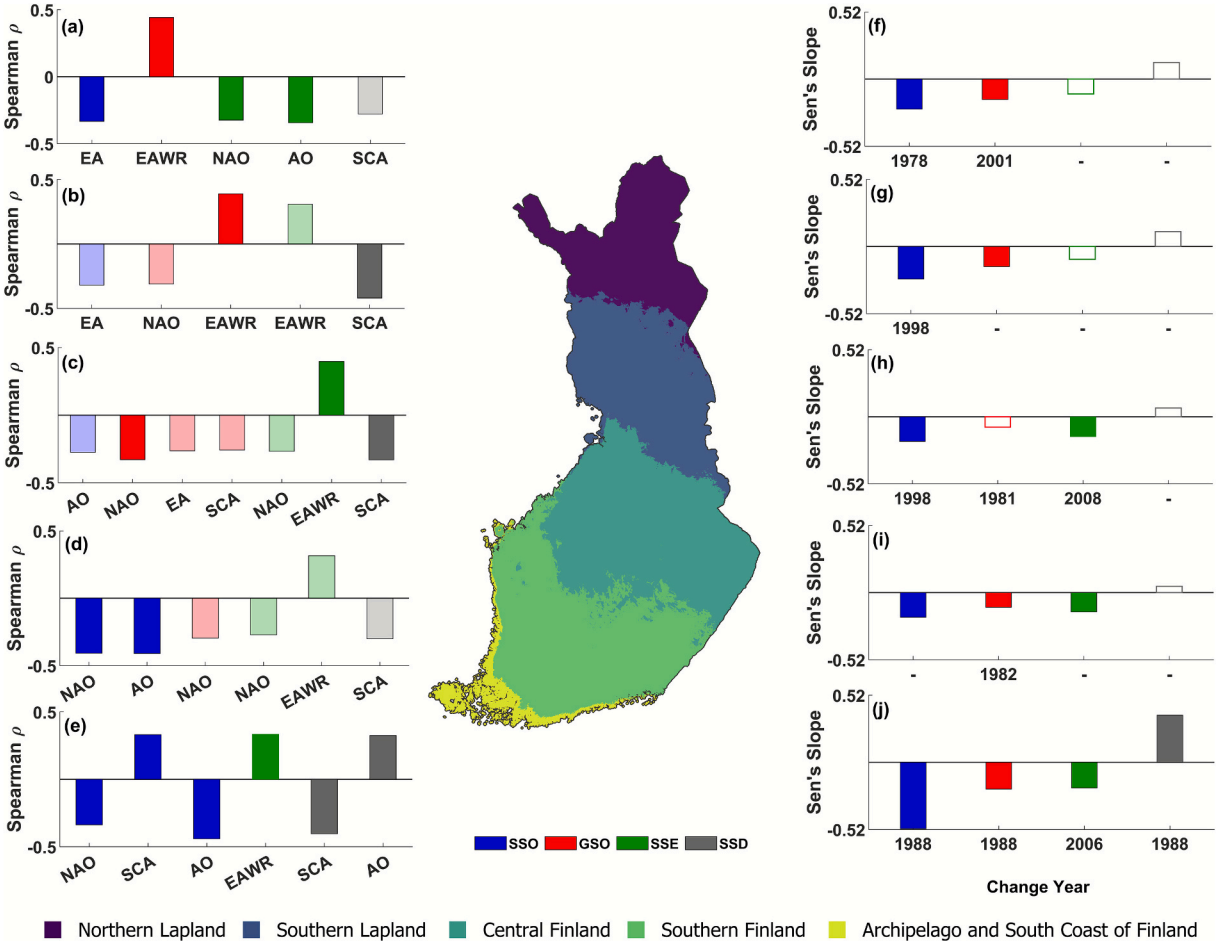

Fig. 7. Associations of spring timing indices with TCPs, their trends, and change points across clusters. (a–e) Correlation coefficients between spring timing indices and TCPs within clusters. (f–j) Slopes of change (day/year) and change points for each spring timing index within clusters. Panels correspond to: (a,f) Northern Lapland, (b,g) Southern Lapland, (c,h) Central Finland, (d,i) Southern Finland, and (e,j) the Archipelago and South Coast clusters. Dark bars indicate significant correlations at $p < 0.01$, light bars indicate correlations at $p < 0.05$, and hollow bars indicate no significant trends. The x-axis in panels (f–j) shows change points identified by the Pettitt test; dashes indicate the absence of statistically significant change points.

4. Discussion

Seasonal cycles in boreal regions are changing more rapidly than in most other parts of the world. Although there is a broad consensus that climate change is driving these shifts, characterizing the variability associated with atmospheric teleconnection patterns remains essential for identifying the drivers of abnormal seasonal changes. Given its ecological and societal importance and sensitivity to climate, this study focused on spring season timing changes in the boreal region.

The results of this study show clear evidence of an overall trend toward an earlier onset of spring in the boreal region, consistent with previous studies focusing on hydrological and ecological variables (Blåfield et al., 2024; Lintunen et al., 2024; Helama et al., 2020; Luomaranta et al., 2014). By applying specific thermal timing indices across Finland, this study shows that the start, midpoint, and end of the spring season have advanced, accompanied by an overall increase in duration. Based on a wide scientific evidence (Intergovernmental Panel on Climate Change (IPCC), 2023) and studies reporting earlier onset of the thermal growing season in Finland (Helama et al., 2020; Irannezhad and Kløve, 2015), this long-term shift in the spring timing is likely attributable to anthropogenic global warming.

Findings from this study across Finland reveal considerable regional variation in spring timing trends, with distinct clusters identified in the timing indices. The regional clusters demonstrate how different physical characteristics affect the similarity of thermal seasons across regions: The Southern Finland cluster showed a relatively long SSD of 53 days, while the Central Finland cluster exhibited a shorter and more consistent SSD of 47 days (standard deviation = 1.9), even though both clusters are lake-dominated which strongly influence the ecological and hydrological processes of the region (Pöysä, 2022). We also found that the Southern Lapland cluster, extending toward the Bothnian coast, reflects the influence of prolonged sea ice cover, which delays coastal warming and aligns its phenology with inland northern regions (Finnish Meteorological Institute, 2025b).

The results indicate that a significant increase in SSD is evident in both northern Finland and the southwestern archipelago; this lengthening suggests that the SSO advanced more strongly than SSE. Notably, this finding aligns with projections that suggest an extended spring duration in the region under future climate scenarios (Ruosteenoja et al., 2020). According to long-term trends, the SSD in southwestern Finland and the surrounding archipelago shows a significant change, extending by nearly six days per decade. This noticeable shift parallels the greatest increases in growing season length recorded at stations along the Baltic Sea coast (Linderholm et al., 2008). The regional analysis conducted in this study reveals that spring in southwestern Finland and the surrounding archipelago exhibits the longest durations and the greatest spatial variability. The pronounced spatial variability is likely influenced by frequent and increasing temperature fluctuations around 0 °C at lower latitudes (Aalto et al., 2023; Freistetter et al., 2022), meaning that even small temperature changes can substantially affect both SSO

and SSD. In addition, proximity to the sea is an important factor influencing the timing of spring in the region. For example, the Baltic Sea has been characterized as having highly regular and seasonally variable water temperature patterns that can influence the coastal zone, with the strongest sea effects observed in spring and autumn (Veneranta et al., 2016; Väyrynen et al., 2017). This conclusion is further supported by Lintunen et al. (2024), who found that spring floods have advanced particularly along Finland's coastal areas. The Northern Lapland cluster also exhibits similarly high spatial variability of SSD, where summers are cooler and shorter (De Castro et al., 2007), and fluctuations around the 10 °C threshold are more frequent, which in turn explain the greater variability in the SSE and therefore the SSD as well. In addition to latitude, altitude may also be an influential factor, as northern Lapland in Finland has higher elevations compared to the rest of the country. Previous studies have similarly linked seasonal timing to topographic and latitudinal gradients (Deng et al., 2019; Ziska et al., 2011).

Although the findings offer clear evidence that spring timing variability and long-term trends are linked to latitude, altitude, and proximity to the sea, spring timing in the boreal zone also appears to be closely connected to multiple teleconnection patterns. Analysis of the data revealed significant relationships between large-scale atmospheric oscillations and the timing of spring events in Finland, based on both national-scale and cluster-based analysis. For example, the NAO appeared to drive earlier SSO, GSO, and SSE. Similarly, the AO showed a strong association with earlier SSO, suggesting that the positive phases of NAO and AO, which are typically associated with milder winters in northern Europe (Myoung et al., 2017; Hurrell and Van Loon, 1997; Thompson and Wallace, 2001), lead to earlier spring occurrences and an accelerated snow melt process in the boreal area. The cluster analysis showed similar results; however, it also indicated that these two teleconnection patterns were more influential for SSO in the southern clusters and for SSE in the Northern Lapland cluster, while the NAO was mainly influential for GSO in the central region.

On the other hand, we found that regional atmospheric blocking associated with positive phases of the SCA was connected to delayed spring. Previous studies have shown that positive SCA phases during winter and spring are often linked to lower regional temperatures (Bueh and Nakamura, 2007), which can, in turn, delay biological responses such as animal migration (Gołębiewski and Remisiewicz, 2023). The positive phase of the SCA is also associated with positive summer temperature anomalies over the Scandinavian region (Dutton, 2021). In this study, these contrasting winter–summer temperature anomalies under strong positive SCA phases were found to be strongly linked to a shorter thermal spring season. This relationship was confirmed by the cluster analysis, which revealed a connection between SSD and SCA across all clusters, with more notable influences in southern Lapland, the central region, and the archipelago area.

The results suggest that the EAWR pattern is a key driver of the GSO and SSE, with its anomalies associated with delays in both. Earlier studies support these results, as the positive phase of the EAWR has been linked to colder conditions over western Russia and eastern Europe (Ceglar et al., 2017; CPC, 2012). The cluster correlation analysis showed that the EAWR primarily influences GSO timing in northern and southern Lapland, and SSE timing in the central and southernmost clusters.

Additionally, the analysis of this study indicated that spring timing indices have experienced a pronounced shift, particularly since the 1980s; this observation aligns with findings by Kaukoranta and Hakala (2008), who documented a similar acceleration in temperature-derived growing season in Finland during the 1980s. The regional time series derived from each cluster also revealed distinct change points during the 1980s and 1990s. During these decades, all indices except SSE exhibited noticeable shifts in their respective temporal patterns. Although the Pettitt test detected change points in the time series, a key limitation of this method is that it can identify only a single change point, thereby partitioning the record into just two temporal periods (Guilpart et al., 2021). Consequently, future research would benefit from applying methods capable of detecting multiple change points to better characterize the structure of climate fluctuations and regime transitions.

In summary, the results indicate that environmental factors, anthropogenic climate change, and large-scale teleconnection patterns collectively shape the timing and variability of the spring season across the boreal study area. However, disentangling the relative influence of anthropogenic climate change from that of teleconnection patterns remains challenging, and it is uncertain whether these drivers can be fully separated in terms of their effects on spring timing dynamics. The results revealed change points in the time series of spring timing indices around the 1980s and 1990s, which may be associated with shifts in teleconnection patterns, as several studies have reported changes in the dominant phases of the large-scale atmospheric patterns during the same periods (Gong et al., 2024; Wu et al., 2022; Yeager and Danabasoglu, 2014). For example, the winter NAO experienced a major shift in the early 1990s, while the Pacific center intensity of the AO exhibited multidecadal fluctuations, with low amplitude before 1980, a peak from 1980 to 2000, and a sharp decline following 2000 (Wu et al., 2022; Gong et al., 2024). On the other hand, the impacts of anthropogenic climate change have been detected globally during this period (Li et al., 2025; Reid et al., 2016), suggesting that the observed shifts in spring timing indices may be partly attributable to climate change. In addition, recent evidence indicates that anthropogenic warming can alter atmospheric teleconnections in the Northern Hemisphere, potentially contributing to these changes. For example, a recent study showed that global warming amplifies the variability of the summer North Atlantic Oscillation, thereby increasing the likelihood of extreme phases (Liu et al., 2025). Another study suggested that warming of the Indian Ocean sea surface temperatures is linked to the positive trend of the AO (Jeong et al., 2022). These findings suggest that the influence of climate change on the evolving behavior of atmospheric patterns may also play a critical role in shaping the timing of thermal seasons, and should therefore be a focus of future research.

5. Conclusions

This study provides an assessment of the boreal thermal spring season, emphasizing its links to atmospheric teleconnections, geographical drivers, and anthropogenic climate change. Using six decades of high-resolution temperature observations from Finland, the analysis offers insights into the mechanisms driving spring timing variability. The results demonstrate that the proposed approach captures the influence of climate change and large-scale atmospheric patterns on both long-term trends and interannual variability of the thermal spring season, and provides a framework that can be applied in similar studies across other regions.

Results of the trend analysis over 6 decades reveal earlier spring onset and a prolonged spring season in the region, which can be associated with rising global temperatures. Interannual variability is largely driven by large-scale atmospheric patterns, whereas geographical features shape the spatial distribution of spring dynamics.

During the study period, the spring season in Finland has lengthened by 3–6 days per decade, particularly in northern regions and along the southwestern coast. Spring timing has advanced across the entire study area, with the strongest trends observed in spring onset, which has advanced by 6 days per decade in the southwestern archipelago. Substantial spatial variability in spring timing indices was observed across the region, primarily driven by latitudinal gradients, where temperatures often hovered near critical thresholds, amplifying variability in the onset, end, and duration of spring. Additionally, proximity to the Baltic Sea has influenced regional responses.

The interannual variability of the spring season was linked to large-scale atmospheric patterns. Early spring onset was associated with the positive phase of the Arctic Oscillation (AO), while delayed spring end and delayed onset of the growing season were linked to the positive

phase of the East Atlantic–West Russia (EAWR) pattern. An early start of the growing season was associated with the positive phase of the North Atlantic Oscillation (NAO), and the shorter duration of the thermal spring season showed a connection to the positive phase of the Scandinavian (SCA) pattern.

These results demonstrate that the boreal spring has both advanced and lengthened, influenced by geographic factors, global warming, and large-scale atmospheric drivers. The socio-economic implications of an earlier and prolonged boreal spring are likely to vary substantially across regions, underscoring the importance of identifying where adaptation measures should be prioritized. In addition, further research is needed to explain the factors behind the variability of teleconnection patterns, such as the potential influence of climate change.

CRediT authorship contribution statement

Sadegh Kaboli: Visualization, Validation, Software, Methodology, Investigation, Formal analysis, Data curation, Writing – review & editing, Writing – original draft. **Ville Kankare:** Supervision, Conceptualization, Writing – review & editing. **Ali Torabi Haghighi:** Methodology, Conceptualization, Writing – review & editing. **Cintia Bertacchi Uvo:** Methodology, Conceptualization, Writing – review & editing. **Elina Kasvi:** Supervision, Methodology, Funding acquisition, Conceptualization, Writing – review & editing.

Declaration of Generative AI and AI-assisted technologies in the writing process

During the preparation of this work the authors used ChatGPT in order to improve the linguistic clarity and readability of the manuscript. After using this tool/service, the authors reviewed and edited the content as needed and take full responsibility for the content of the publication.

Declaration of competing interest

The authors declare that they have no known competing financial interests or personal relationships that could have appeared to influence the work reported in this paper.

Acknowledgments

This study has been co-funded by the European Union's Horizon Europe research and innovation programme under the Marie Skłodowska-Curie Actions grant agreement No. 101125250 (UTU-GreDiT program). The work was also supported by the Research Council of Finland via the Digital Waters Flagship (decision no. 359247) and the AnthroCliMocs-project (decision no. 355018). Parts of the calculations were performed using the CSC supercomputer Puhti provided by the CSC—IT Center of Science, Finland. We gratefully acknowledge their computational resources.

Appendix A. Supplementary data

Supplementary data to this article can be found online at https://doi.org/10.1016/j.atmosres.2026.108752.

Data availability

Grid-based daily mean temperature, latitude, and longitude data were obtained from the Finnish Meteorological Institute (FMI) via their gridded observational dataset (https://en.ilmatieteenlaitos.fi/gridded-observations-on-aws-s3). Monthly TCP indices for the period 1961–2023 were sourced from the Climate Prediction Center (CPC) of the National Oceanic and Atmospheric Administration (https://ftp.cpc.ncep.noaa.gov/wd52dg/data/indices/tele_index.nh). The distance from the sea was calculated using global coastline data provided by the Flanders Marine Institute (doi: 10.14284/542). Terrain elevation data at a spatial resolution of 90 m were obtained from the Copernicus Global Digital Elevation Model via the OpenTopography platform (doi: https://doi.org/10.5069/G9028PQB) and subsequently resampled to 1000 m to align with the spatial resolution used in this study. Supporting output maps and datasets generated from this study are available in the Zenodo repository (doi: https://doi.org/10.5281/zenodo.15797041). In this study, MATLAB 2024a, particularly the Statistics and Machine Learning Toolbox, was employed for data processing, index calculation, trend analysis, and clustering. We utilized the 'sklearn.metrics' Python package and the 'silhouette_samples' and 'silhouette_score' functions to calculate silhouette scores. QGIS Desktop version 3.34.8 was used for map visualization and measuring grid distances from the sea. Spearman correlation analysis, with 10,000 bootstrap samples, was performed using IBM SPSS Statistics version 29.0.20.

References

Aalto, J., Pirinen, P., Jylhä, K., 2016. New gridded daily climatology of Finland: Permutation-based uncertainty estimates and temporal trends in climate. J. Geophys. Res.-Atmos. 121, 3807–3823. https://doi.org/10.1002/2015JD024651.

Aalto, J., Pirinen, P., Kauppi, P.E., Rantanen, M., Lussana, C., Lyytikäinen-Saarenmaa, P., Gregow, H., 2022. High-resolution analysis of observed thermal growing season variability over northern Europe. Clim. Dyn. 58, 1477–1493. https://doi.org/10.1007/s00382-021-05970-y.

Aalto, J., Lehtonen, I., Pirinen, P., Aapala, K., Heikkinen, R.K., 2023. Bioclimate change across the protected area network of Finland. Sci. Total Environ. 893, 164782. https://doi.org/10.1016/j.scitotenv.2023.164782.

Ault, T.R., Macalady, A.K., Pederson, G.T., Betancourt, J.L., Schwartz, M.D., 2011. Northern Hemisphere Modes of Variability and the timing of Spring in Western North America. J. Clim. 24, 4003–4014. https://doi.org/10.1175/2011JCLI4069.1.

Barnston, A.G., Livezey, R.E., 1987. Classification, Seasonality and Persistence of Low-Frequency Atmospheric Circulation patterns. Mon. Weather Rev. 115, 1083–1126. https://doi.org/10.1175/1520-0493(1987)115<1083:CSAPOL>2.0.CO;2.

Blåfield, L., Marttila, H., Kasvi, E., Alho, P., 2024. Temporal shift of hydroclimatic regime and its influence on migration of a high latitude meandering river. J. Hydrol. 633, 130935. https://doi.org/10.1016/j.jhydrol.2024.130935.

Bueh, C., Nakamura, H., 2007. Scandinavian pattern and its climatic impact. Q. J. R. Meteorol. Soc. 133, 2117–2131. https://doi.org/10.1002/qj.173.

Cayan, D.R., Dettinger, M.D., Kammerdiener, S.A., Caprio, J.M., Peterson, D.H., 2001. Changes in the Onset of Spring in the Western United States. Bull. Am. Meteorol. Soc. 82, 399–415. https://doi.org/10.1175/1520-0477(2001)082<0399:CITOOS>2.3.CO;2.

Ceglar, A., Turco, M., Toreti, A., Doblas-Reyes, F.J., 2017. Linking crop yield anomalies to large-scale atmospheric circulation in Europe. Agric. For. Meteorol. 240–241, 35–45. https://doi.org/10.1016/j.agrformet.2017.03.019.

Cornes, R.C., Van Der Schrier, G., Squintu, A.A., 2019. A reappraisal of the thermal growing season length across Europe. Int. J. Climatol. 39, 1787–1795. https://doi.org/10.1002/joc.5913.

CPC, 2012. Climate prediction center—Polar/Eurasia. NOAA Cent. Weather Clim. Predict. https://www.cpc.ncep.noaa.gov/data/teledoc/poleur.shtml (accessed 3.3.25).

De Castro, M., Gallardo, C., Jylha, K., Tuomenvirta, H., 2007. The use of a climate-type classification for assessing climate change effects in Europe from an ensemble of nine regional climate models. Clim. Chang. 81, 329–341. https://doi.org/10.1007/s10584-006-9224-1.

Deng, C., Bai, H., Gao, S., Zhao, T., Ma, X., 2019. Differences and variations in the elevation-dependent climatic growing season of the northern and southern slopes of the Qinling Mountains of China from 1985 to 2015. Theor. Appl. Climatol. 137, 1159–1169. https://doi.org/10.1007/s00704-018-2654-7.

Dutton, J., 2021. What is the scandinavian pattern climate index? World Clim. Serv. https://www.worldclimateservice.com/2021/09/06/scandinavian-pattern/ (accessed 8.15.25).

Fabiano, F., Christensen, H.M., Strommen, K., Athanasiadis, P., Baker, A., Schiemann, R., Corti, S., 2020. Euro-Atlantic weather Regimes in the PRIMAVERA coupled climate simulations: impact of resolution and mean state biases on model performance. Clim. Dyn. 54, 5031–5048. https://doi.org/10.1007/s00382-020-05271-w.

Finnish Meteorological Institute, 2025a. Seasons in Finland. https://en.ilmatieteenlaitos.fi/seasons-in-finland (accessed 4.3.25).

Finnish Meteorological Institute, 2025b. Ice season in the Baltic Sea. Finn. Meteorol. Inst. https://en.ilmatieteenlaitos.fi/ice-season-in-the-baltic-sea (accessed 5.3.25).

Freistetter, N.-C., Médus, E., Hippi, M., Kangas, M., Dobler, A., Belušić, D., Käyhkö, J., Partanen, A.-I., 2022. Climate change impacts on future driving and walking conditions in Finland, Norway and Sweden. Reg. Environ. Chang. 22, 58. https://doi.org/10.1007/s10113-022-01920-4.

Ghag, K.S., Ahrari, A., Panchanathan, A., Mustafa, S.M.T., Liedes, T., Klöve, B., Haghighi, A.T., 2024. Effect of long-term climate signatures on regional and local

potato yield in Finland. Smart Agric. Technol. 7, 100411. https://doi.org/10.1016/j.atech.2024.100411.
Gołębiewski, I., Remisiewicz, M., 2023. Carry-over effects of climate variability at breeding and non-breeding grounds on spring migration in the European Wren Troglodytes troglodytes at the Baltic Coast. Animals 13, 2015. https://doi.org/10.3390/ani13122015.
Gong, H., Ma, K., Liu, B., Cohen, J., Wang, L., 2024. Structural fluctuations of the Arctic Oscillation tied to the Atlantic Multidecadal Oscillation. Npj Clim. Atmospheric Sci. 7. https://doi.org/10.1038/s41612-024-00805-z.
Greene, C.A., Thirumalai, K., Kearney, K.A., Delgado, J.M., Schwanghart, W., Wolfenbarger, N.S., Thyng, K.M., Gwyther, D.E., Gardner, A.S., Blankenship, D.D., 2019. The climate data toolbox for MATLAB. Geochem. Geophys. Geosyst. 20, 3774–3781. https://doi.org/10.1029/2019GC008392.
Guilpart, E., Espanmanesh, V., Tilmant, A., Anctil, F., 2021. Combining split-sample testing and hidden Markov modelling to assess the robustness of hydrological models. Hydrol. Earth Syst. Sci. 25, 4611–4629. https://doi.org/10.5194/hess-25-4611-2021.
Hekmatzadeh, A.A., Kaboli, S., Torabi Haghighi, A., 2020. New indices for assessing changes in seasons and in timing characteristics of air temperature. Theor. Appl. Climatol. 140, 1247–1261. https://doi.org/10.1007/s00704-020-03156-w.
Helama, S., Tolvanen, A., Karhu, J., Poikolainen, J., Kubin, E., 2020. Finnish National Phenological Network 1997–2017: from observations to trend detection. Int. J. Biometeorol. 64, 1783–1793. https://doi.org/10.1007/s00484-020-01961-6.
Hurrell, J.W., 1995. Decadal Trends in the North Atlantic Oscillation: Regional Temperatures and Precipitation. Science 269, 676–679. https://doi.org/10.1126/science.269.5224.676.
Hurrell, J.W., Van Loon, H., 1997. Decadal variations in climate associated with the North Atlantic oscillation. Clim. Chang. 36, 301–326. https://doi.org/10.1023/a:1005314315270.
Intergovernmental Panel on Climate Change (IPCC), 2023. Summary for Policymakers. In: Climate Change 2021 – The Physical Science Basis: Working Group I Contribution to the Sixth Assessment Report of the Intergovernmental Panel on Climate Change. Cambridge University Press, pp. 3–32. https://doi.org/10.1017/9781009157896.001.
Irannezhad, M., Kløve, B., 2015. Do atmospheric teleconnection patterns explain variations and trends in thermal growing season parameters in Finland? Int. J. Climatol. 35, 4619–4630. https://doi.org/10.1002/joc.4311.
Irannezhad, M., Ahmadi, B., Kløve, B., Moradkhani, H., 2017. Atmospheric circulation patterns explaining climatological drought dynamics in the boreal environment of Finland, 1962–2011. Int. J. Climatol. 37, 801–817. https://doi.org/10.1002/joc.5039.
Jaagus, J., Truu, J., Ahas, R., Aasa, A., 2003. Spatial and temporal variability of climatic seasons on the east European Plain in relation to large-scale atmospheric circulation. Clim. Res. 23, 111–129. https://doi.org/10.3354/cr023111.
Jeong, Y.-C., Yeh, S.-W., Lim, Y.-K., Santoso, A., Wang, G., 2022. Indian Ocean warming as key driver of long-term positive trend of Arctic Oscillation. Npj Clim. Atmospheric Sci. 5. https://doi.org/10.1038/s41612-022-00279-x.
Jo, A.R., Lee, J., Sharma, S., Lee, S., 2024. Season-dependent atmosphere-ocean coupled processes driving SST seasonality changes in a warmer climate. Geophys. Res. Lett. 51. https://doi.org/10.1029/2023GL106953 e2023GL106953.
Kaboli, S., Hekmatzadeh, A.A., Darabi, H., Haghighi, A.T., 2021. Variation in physical characteristics of rainfall in Iran, determined using daily rainfall concentration index and monthly rainfall percentage index. Theor. Appl. Climatol. 144, 507–520. https://doi.org/10.1007/s00704-021-03553-9.
Kaukoranta, T., Hakala, K., 2008. Impact of spring warming on sowing times of cereal, potato and sugar beet in Finland. Agric. Food Sci. 17, 165. https://doi.org/10.2137/145960608785328198.
Kendall, M.G., 1957. Rank correlation methods. Biometrika 44, 298. https://doi.org/10.2307/2333282.
Kiani, S., Irannezhad, M., Ronkanen, A.-K., Moradkhani, H., Kløve, B., 2018. Effects of recent temperature variability and warming on the Oulu-Hailuoto ice road season in the northern Baltic Sea. Cold Reg. Sci. Technol. 151, 1–8. https://doi.org/10.1016/j.coldregions.2018.02.010.
Kuschnerus, M., Lindenbergh, R., Vos, S., 2021. Coastal change patterns from time series clustering of permanent laser scan data. Earth Surf. Dyn. 9, 89–103. https://doi.org/10.5194/esurf-9-89-2021.
Li, Y., Duan, W., Zeng, Z., Zou, S., Wang, X., Zhu, Z., Zhu, E., Wang, J., 2025. Asynchronous abrupt warming across Eurasia since the 1980s. Npj Clim. Atmos. Sci. 8. https://doi.org/10.1038/s41612-025-01209-3.
Lin, W., Wang, C., 2022. Longer summers in the Northern Hemisphere under global warming. Clim. Dyn. 58, 2293–2307. https://doi.org/10.1007/s00382-021-06009-y.
Lin, M., Hou, L., Qi, Z., Wan, L., 2022. Impacts of climate change and human activities on vegetation NDVI in China's Mu Us Sandy Land during 2000–2019. Ecol. Indic. 142, 109164. https://doi.org/10.1016/j.ecolind.2022.109164.
Linderholm, H.W., Walther, A., Chen, D., 2008. Twentieth-century trends in the thermal growing season in the Greater Baltic Area. Clim. Chang. 87, 405–419. https://doi.org/10.1007/s10584-007-9327-3.
Linkosalo, T., Häkkinen, R., Terhivuo, J., Tuomenvirta, H., Hari, P., 2009. The time series of flowering and leaf bud burst of boreal trees (1846–2005) support the direct temperature observations of climatic warming. Agric. For. Meteorol. 149, 453–461. https://doi.org/10.1016/j.agrformet.2008.09.006.
Lintunen, K., Kasvi, E., Uvo, C.B., Alho, P., 2024. Changes in the discharge regime of Finnish rivers. J. Hydrol. Reg. Stud. 53, 101749. https://doi.org/10.1016/j.ejrh.2024.101749.
Liu, Q., Bader, J., Jungclaus, J.H., Matei, D., 2025. More extreme summertime North Atlantic Oscillation under climate change. Commun. Earth Environ. 6, 474. https://doi.org/10.1038/s43247-025-02422-x.
Lloyd, S., 1982. Least squares quantization in PCM. IEEE Trans. Inf. Theory 28, 129–137. https://doi.org/10.1109/TIT.1982.1056489.
Lorenz, E.N., 1956. Empirical Orthogonal Functions and Statistical Weather Prediction (No. Statistical Forecast Project Report 1). Department of Meteorology, MIT.
Luomaranta, A., Ruosteenoja, K., Jylhä, K., Gregow, H., Haapala, J., Laaksonen, A., 2014. Multimodel estimates of the changes in the Baltic Sea ice cover during the present century. Tellus Dyn. Meteorol. Oceanogr. 66, 22617. https://doi.org/10.3402/tellusa.v66.22617.
Luomaranta, A., Aalto, J., Jylhä, K., 2019. Snow cover trends in Finland over 1961–2014 based on gridded snow depth observations. Int. J. Climatol. 39, 3147–3159. https://doi.org/10.1002/joc.6007.
MacQueen, J.B., 1967. Some methods of classification and analysis of multivariate observations. In: Proc. of 5th Berkeley Symposium on Math. Stat. and Prob, pp. 281–298.
Mann, H.B., 1945. Nonparametric Tests against Trend. Econometrica 13, 245. https://doi.org/10.2307/1907187.
Myoung, B., Kim, S.H., Kim, J., Kafatos, M.C., 2017. On the Relationship between Spring NAO and Snowmelt in the Upper Southwestern United States. J. Clim. 30, 5141–5149. https://doi.org/10.1175/JCLI-D-16-0239.1.
Naderian, D., Noori, R., Bateni, S.M., Jun, C., Kim, D., Shahmohammad, M., Alizadeh, F., Kianmehr, P., Woolway, R.I., 2025. Pivotal role of snow depth, local atmospheric conditions, and large-scale climate signals on ice thinning in Finnish lakes. Sci. Total Environ. 966, 178715. https://doi.org/10.1016/j.scitotenv.2025.178715.
North, G.R., Bell, T.L., Cahalan, R.F., Moeng, F.J., 1982. Sampling Errors in the Estimation of Empirical Orthogonal Functions. Mon. Weather Rev. 110, 699–706. https://doi.org/10.1175/1520-0493(1982)110<0699:SEITEO>2.0.CO;2.
Okkonen, J., Kløve, B., 2010. A conceptual and statistical approach for the analysis of climate impact on ground water table fluctuation patterns in cold conditions. J. Hydrol. 388, 1–12. https://doi.org/10.1016/j.jhydrol.2010.02.015.
Olsson, T., Jakkila, J., Veijalainen, N., Backman, L., Kaurola, J., Vehviläinen, B., 2015. Impacts of climate change on temperature, precipitation and hydrology in Finland – studies using bias corrected Regional climate Model data. Hydrol. Earth Syst. Sci. 19, 3217–3238. https://doi.org/10.5194/hess-19-3217-2015.
Parmesan, C., 2006. Ecological and Evolutionary responses to recent climate Change. Annu. Rev. Ecol. Evol. Syst. 37, 637–669. https://doi.org/10.1146/annurev.ecolsys.37.091305.110100.
Pettitt, A.N., 1979. A Non-Parametric Approach to the Change-Point Problem. Appl. Stat. 28, 126. https://doi.org/10.2307/2346729.
Pirinen, P., Simola, H., Aalto, J., Kaukoranta, J.-P., Karlsson, P., Ruuhela, R., 2012. Climatological Statistics of Finland 1981–2010 (No. Reports 2012:1). Finnish Meteorological Institute, Helsinki.
Pöysä, H., 2022. Local variation in the timing and advancement of lake ice breakup and impacts on settling dynamics in a migratory waterbird. Sci. Total Environ. 811, 151397. https://doi.org/10.1016/j.scitotenv.2021.151397.
Reid, P.C., Hari, R.E., Beaugrand, G., Livingstone, D.M., Marty, C., Straile, D., Barichivich, J., Goberville, E., Adrian, R., Aono, Y., Brown, R., Foster, J., Groisman, P., Hélaouët, P., Hsu, H., Kirby, R., Knight, J., Kraberg, A., Li, J., Lo, T., Myneni, R.B., North, R.P., Pounds, J.A., Sparks, T., Stübi, R., Tian, Y., Wiltshire, K. H., Xiao, D., Zhu, Z., 2016. Global impacts of the 1980s regime shift. Glob. Chang. Biol. 22, 682–703. https://doi.org/10.1111/gcb.13106.
Ren, Y., Qiu, J., Zeng, Z., Liu, X., Sitch, S., Pilegaard, K., Yang, T., Wang, S., Yuan, W., Jain, A.K., 2024. Earlier spring greening in Northern Hemisphere terrestrial biomes enhanced net ecosystem productivity in summer. Commun. Earth Environ. 5, 122. https://doi.org/10.1038/s43247-024-01270-5.
Rousseeuw, P.J., 1987. Silhouettes: a graphical aid to the interpretation and validation of cluster analysis. J. Comput. Appl. Math. 20, 53–65. https://doi.org/10.1016/0377-0427(87)90125-7.
Ruosteenoja, K., Räisänen, J., Venäläinen, A., Kämäräinen, M., 2016. Projections for the duration and degree days of the thermal growing season in Europe derived from CMIP5 model output. Int. J. Climatol. 36, 3039–3055. https://doi.org/10.1002/joc.4535.
Ruosteenoja, K., Markkanen, T., Räisänen, J., 2020. Thermal seasons in northern Europe in projected future climate. Int. J. Climatol. 40, 4444–4462. https://doi.org/10.1002/joc.6466.
Schwartz, M.D., Ahas, R., Aasa, A., 2006. Onset of spring starting earlier across the Northern Hemisphere. Glob. Chang. Biol. 12, 343–351. https://doi.org/10.1111/j.1365-2486.2005.01097.x.
Seidl, R., Thom, D., Kautz, M., Martin-Benito, D., Peltoniemi, M., Vacchiano, G., Wild, J., Ascoli, D., Petr, M., Honkaniemi, J., Lexer, M.J., Trotsiuk, V., Mairota, P., Svoboda, M., Fabrika, M., Nagel, T.A., Reyer, C.P.O., 2017. Forest disturbances under climate change. Nat. Clim. Chang. 7, 395–402. https://doi.org/10.1038/nclimate3303.
Sen, P.K., 1968. Estimates of the Regression Coefficient based on Kendall's Tau. J. Am. Stat. Assoc. 63, 1379–1389. https://doi.org/10.1080/01621459.1968.10480934.
Serinaldi, F., Kilsby, C.G., 2016. The importance of prewhitening in change point analysis under persistence. Stoch. Env. Res. Risk A. 30, 763–777. https://doi.org/10.1007/s00477-015-1041-5.
Sobral, B.S., Oliveira-Júnior, J.F.D., De Gois, G., Pereira-Júnior, E.R., Terassi, P.M.D.B., Muniz-Júnior, J.G.R., Lyra, G.B., Zeri, M., 2019. Drought characterization for the state of Rio de Janeiro based on the annual SPI index: trends, statistical tests and its relation with ENSO. Atmos. Res. 220, 141–154. https://doi.org/10.1016/j.atmosres.2019.01.003.

Thompson, D.W.J., Wallace, J.M., 1998. The Arctic oscillation signature in the wintertime geopotential height and temperature fields. Geophys. Res. Lett. 25, 1297–1300. https://doi.org/10.1029/98GL00950.

Thompson, D.W.J., Wallace, J.M., 2001. Regional climate Impacts of the Northern Hemisphere Annular Mode. Science 293, 85–89. https://doi.org/10.1126/science.1058958.

Vaitkuviene, D., Dagys, M., Bartkeviciene, G., Romanovskaja, D., 2015. The effect of weather variables on the White Stork (Ciconia ciconia) spring migration phenology. Ornis Fenn. 92. https://doi.org/10.51812/of.133867.

Väyrynen, R., Suomi, J., Käyhkö, J., 2017. Fine-scale analysis of sea effect on coastal air temperatures at different time scales. Boreal Environ. Res. 22, 369.

Veneranta, L., Vanhatalo, J., Urho, L., 2016. Detailed temperature mapping–Warming characterizes archipelago zones. Estuar. Coast. Shelf Sci. 182, 123–135. https://doi.org/10.1016/j.ecss.2016.09.011.

Wu, X., Che, T., Li, X., Wang, N., Yang, X., 2018. Slower snowmelt in spring along with climate warming across the Northern Hemisphere. Geophys. Res. Lett. 45. https://doi.org/10.1029/2018GL079511.

Wu, R., Dai, P., Chen, S., 2022. Persistence or transition of the North Atlantic Oscillation across Boreal Winter: role of the North Atlantic Air-Sea Coupling. J. Geophys. Res.-Atmos. 127. https://doi.org/10.1029/2022jd037270.

Yeager, S., Danabasoglu, G., 2014. The origins of late-twentieth-century variations in the large-Scale North Atlantic Circulation. J. Clim. 27, 3222–3247. https://doi.org/10.1175/jcli-d-13-00125.1.

Yue, S., Pilon, P., Phinney, B., Cavadias, G., 2002. The influence of autocorrelation on the ability to detect trend in hydrological series. Hydrol. Process. 16, 1807–1829.

Zhang, Y., Moges, S., Block, P., 2016. Optimal cluster analysis for objective regionalization of seasonal precipitation in regions of high spatial–temporal variability: application to Western Ethiopia. J. Clim. 29, 3697–3717. https://doi.org/10.1175/JCLI-D-15-0582.1.

Zhao, W., Gao, B., Deng, J., Sun, J., Chen, L., Fan, S., 2024. Study on the characteristics of urban background ozone pollution based on long-term observations from mountain sites in China during 2015–2022. Atmos. Res. 311, 107696. https://doi.org/10.1016/j.atmosres.2024.107696.

Zhu, K., Chen, W., Hu, P., Luo, Y., Yang, R., Jiang, L., Cai, Q., Gao, L., Li, J., Peng, Y., Wu, C., Niu, Z., 2025. Observational climatology and interannual variability of the spring rainy season onset over southern China: Objective definition and influence from tropical Pacific Ocean. Atmos. Res. 320, 108030. https://doi.org/10.1016/j.atmosres.2025.108030.

Ziska, L., Knowlton, K., Rogers, C., Dalan, D., Tierney, N., Elder, M.A., Filley, W., Shropshire, J., Ford, L.B., Hedberg, C., Fleetwood, P., Hovanky, K.T., Kavanaugh, T., Fulford, G., Vrtis, R.F., Patz, J.A., Portnoy, J., Coates, F., Bielory, L., Frenz, D., 2011. Recent warming by latitude associated with increased length of ragweed pollen season in Central North America. Proc. Natl. Acad. Sci. 108, 4248–4251. https://doi.org/10.1073/pnas.1014107108.